Liang, Y., Zhao, O., Long, Y. and Gardner, L. (2018). Stainless steel channel sections under combined compression and minor axis bending – Part 2: Parametric studies and design. Journal of Constructional Steel Research. In press.

Stainless steel channel sections under combined compression and minor axis bending – Part 2: Parametric studies and design

Yating Liang [a], Ou Zhao [*b], Yue-ling Long [c], Leroy Gardner [d]

[a, b] School of Civil and Environmental Engineering, Nanyang Technological University, 50 Nanyang Avenue, 639798 Singapore, Singapore

[c] School of Civil and Transportation Engineering, Guangdong University of Technology, China

[d] Department of Civil and Environmental Engineering, Imperial College London, London, UK

[*] Corresponding author, Phone: +65 6790 6934

Email: ou.zhao@ntu.edu.sg

Abstract: Following the experimental study and finite element (FE) model validation described in the companion paper, numerical parametric studies and the evaluation of design provisions for stainless steel channel sections under combined axial compressive load and minor axis bending moment are presented herein. The parametric studies were carried out to generate additional structural performance data over a wider range of cross-section aspect ratios and slendernesses, loading combinations and bending orientations. The test data and numerical results have been carefully analysed to develop a comprehensive understanding of the structural performance of stainless steel channel sections under combined compression and minor axis bending moment, and to assess the accuracy of the existing design provisions in Europe and North America. Comparisons of ultimate loads from the tests and FE simulations with the codified resistance predictions revealed that the current design standards typically under-estimate the capacity of stainless steel channel sections under combined compression and minor axis bending moment; this is attributed primarily to the neglect of material strain hardening and the employment of conservative interaction formulae. Improved

design rules featuring more efficient interaction curves, anchored to more precise end points (i.e. cross-section resistances under pure compression and bending moment), are then proposed and presented. The new design proposals are shown to yield both more accurate and more consistent resistance predictions over the existing design provisions. Finally, statistical analyses are presented to confirm the reliability of the new design proposals according to EN 1990.

Keywords: Combined loading; Continuous strength method; Design standards; Parametric studies; Reliability analysis; Stainless steel

1. Introduction

Given the high initial material cost of stainless steels, structural design efficiency is of primary concern. However, many of the provisions in current international structural design standards were developed by mirroring the corresponding carbon steel design rules, without fully accounting for the distinctive nonlinear material response and strain hardening characteristics of stainless steels. As a result, existing stainless steel design standards often yield unduly conservative cross-section resistance predictions, particularly for stocky sections, due to the neglect of the beneficial effect of strain hardening, but can also give inaccurate column and beam-column buckling strength predictions, owing to failure to capture explicitly the detrimental effect of gradual material yielding on member stability [1]. This has prompted research aimed at developing more efficient and accurate design approaches for stainless steel structures. These include the deformation-based continuous strength method (CSM) [2–5] to account for strain hardening and element interaction in the determination of cross-section strengths, and extension of the direct strength method (DSM) [6–8]. In comparison to current

design standards, the CSM has been shown to offer substantially improved capacity predictions for stainless steel cross-sections under both isolated loading (pure compression and pure bending) and combined loading conditions, while DSM yields more accurate and consistent resistance predictions for slender cross-sections.

The present paper focuses on the local cross-section behaviour of stainless steel channel sections subjected to combined compression and minor axis bending moment. Parametric studies are firstly carried out, using the finite element (FE) models validated in the companion paper [9], to generate additional structural performance data. The numerical results derived herein and the test data obtained in the companion paper [9] are then carefully analysed to assess the structural performance of stainless steel channel sections under combined compression and minor axis bending moment in both the 'n' and 'u' orientations, and employed to evaluate the accuracy of the existing design provisions given in the European code EN 1993-1-4 [10] and AISC design guide 27 [11]. Shortcomings of the codified design interaction formulae for stainless steel channel sections under combined loading are highlighted. Finally, improved design rules are proposed, and the applicability and reliability of the new design proposals are evaluated.

2. Numerical parametric studies

Parametric studies were performed, using the numerical models validated in the companion paper [9], to generate additional data, beyond those obtained through experimentation, over a broad range of cross-section geometries, aspect ratios, loading combinations and bending orientations. The derived numerical results are used in Sections 3–5 of the present paper for the evaluation of the design provisions of current international design standards and the

development of new design proposals. In the presented parametric studies, the utilised material properties were taken from the tensile coupon tests on channel section C 40×40×5×5 [9], while the incorporated initial local geometric imperfection pattern was assumed to be of the shape of the lowest elastic buckling mode under the applied loading, with the amplitude determined from the modified Dawson and Walker model [12,13]. Residual stresses were included into the finite element models, according to the distribution pattern shown in the companion paper [9], though previous studies by the authors [9,14] generally indicate relative insensitivity of the local buckling behaviour of stainless steel cross-sections to residual stresses. The geometric dimensions of the modelled channel sections were varied to cover all four cross-section classes, according to the EN 1993-1-4 slenderness limits [10]. Specifically, the outer web widths h were fixed at 100 mm, while the outer flange widths b_f were varied between 33 mm and 100 mm, which resulted in a spectrum of cross-section aspect ratios from 1.0 to 3.0 being considered; the thicknesses of the webs and flanges (t_w and t_f) ranged from 3 mm to 12.5 mm. The lengths of the models L were set to be equal to three times their mean outer cross-section dimension, and the resulting member slendernesses $\overline{\lambda}$ were less than 0.2, to minimise the influence of global buckling. The initial loading eccentricities e_{0e}, defined as the distance from the loading points to the elastic neutral axes of the modelled channel sections, ranged from 1.8 mm and 654 mm, leading to a wide range of axial load-to-bending moment ratios being examined. Minor axis bending moments in both the ‘n’ and ‘u’ orientations were considered. A summary of the modelled stainless steel channel sections under combined axial compression and bending moment about the minor axis is reported in Table 1. In total, 640 parametric study results were generated, with 320 for each bending orientation.

3. Provisions of current international design standards

3.1 General

The current codified design provisions for laser-welded stainless steel channel sections subjected to the combined actions of compression and minor axis bending moment, as given in the European code EN 1993-1-4 [10] and AISC design guide 27 [11], are firstly described and discussed. The accuracy of each design standard is then assessed by comparing the test and numerical failure loads N_u against the predicted failure loads $N_{u,pred}$ [15–18]. The mean $N_u/N_{u,pred}$ ratios for both design codes are shown in Tables 2(a) and 2(b) for stainless steel channel sections under 'n' and 'u' orientation minor axis combined loading conditions, respectively. Note that all the calculations made herein are based on the measured (or modelled) geometric and material properties, and all partial factors are set to be equal to unity, leading to unfactored design strengths being compared.

3.2 European code EN 1993-1-4 (EC3)

The current European code EN 1993-1-4 [10] for stainless steel does not provide specific design rules for cross-section resistances under combined loading, but simply mirrors the corresponding carbon steel provisions given in EN 1993-1-1 [19]. For channel sections subjected to combined compression and bending moment, a linear design interaction formula is employed, as given by Eq. (1), in which N_{Ed} is the design axial compression force, $M_{Ed,z}=N_{Ed}(e_0+e')$ is the design bending moment about the minor axis [15,18,20], where e_0 is the initial loading eccentricity and e' is the mid-height lateral deflection at failure, and N_{Rd} and $M_{z,Rd}$ are the predicted cross-section resistances under pure compression and pure

bending about the minor axis, respectively. Note that the values of e_0, N_{Rd} and $M_{z,Rd}$ depend on the classification of the cross-section. Specifically, for Class 1 and 2 channel sections, where the design neutral axis is assumed to be located at the cross-section plastic neutral axis (PNA), e_0 is taken as the distance from the loading point to the PNA and $M_{z,Rd}$ is equal to the plastic moment capacity $M_{pl,z,Rd}$, defined as the product of the plastic section modulus $W_{pl,z}$ about the minor axis and the 0.2% proof stress $\sigma_{0.2}$; for Class 3 channel sections, where the elastic neutral axis (ENA) is assumed to be the design neutral axis at failure, e_0 is taken as the distance from the loading point to the ENA and $M_{z,Rd}$ reduces to the elastic moment capacity $M_{el,z,Rd}$, defined as the elastic section modulus $W_{el,z}$ multiplied by $\sigma_{0.2}$; for slender Class 4 channel sections, e_0 is equal to the distance from the loading point to the effective neutral axis (EFNA) and $M_{z,Rd}$ is taken as the cross-section effective moment capacity ($M_{eff,z,Rd}=W_{eff,z}\sigma_{0.2}$), with the location of the EFNA and effective section modulus $W_{eff,z}$ determined based on the effective width method in EN 1993-1-4 [10]. With regards to compression resistance N_{Rd}, the values are calculated as the cross-section yield load ($N_{pl,Rd}=A\sigma_{0.2}$) and effective cross-section resistance ($N_{eff,Rd}=A_{eff}\sigma_{0.2}$) for non-slender (Class 1, 2 and 3) and slender (Class 4) channel sections, respectively, where A is gross cross-section area and A_{eff} is the effective cross-section area.

$$\frac{N_{Ed}}{N_{Rd}}+\frac{M_{Ed,z}}{M_{z,Rd}}\leq 1 \tag{1}$$

The experimental and numerical results for the eccentrically loaded stub columns of the different cross-section classes are normalised by the respective cross-section yield loads and plastic moment capacities, and plotted against the average linear design interaction curves obtained from EN 1993-1-4 [10], as shown in Figs 1(a) and 1(b) for the ‘u’ and ‘n’ orientation minor axis combined loading cases, respectively. Note that the $W_{el,z}/W_{pl,z}$ and

$W_{eff,z}/W_{pl,z}$ (i.e. $M_{el,z}/M_{pl,z}$ and $M_{eff,z}/M_{pl,z}$) and A/A_{eff} ratios varied between the modelled sections, and therefore the average linear design interaction curves for Class 3 and 4 channel sections under combined loading are depicted in Figs 1(a) and 1(b). The results generally indicate that the European code EN 1993-1-4 [10] yields rather conservative and scattered capacity predictions for stainless steel channel sections under combined compression and minor axis bending moment in both of the 'n' and 'u' orientations. A quantitative evaluation of the strength predictions from the European code EN 1993-1-4 [10] is reported in Tables 2(a) and 2(b), showing that the mean test (or FE) to EC3 failure load ratios $N_u/N_{u,EC3}$ are equal to 2.31 and 1.85, with coefficients of variation (COV values) equal to 0.27 and 0.14, for stainless steel channel sections under 'u' and 'n' orientation minor axis combined loading, respectively. The conservative and scattered EC3 predictions are attributed to shortcomings in the resistance functions. Specifically, the linear design interaction curve neglects the beneficial stress redistribution that takes place within non-slender channel sections under combined loading, while the compression and bending end points of the design interaction curve are limited to the cross-section yield load and plastic (or elastic and effective) moment resistances, without accounting for the pronounced strain hardening exhibited by stainless steels.

3.3 AISC design guide 27

AISC design guide 27 [11] adopts a bi-linear interaction curve for the design of doubly and singly symmetric stainless steel sections subjected to the combined actions of compression and flexure, as defined by Eqs (2) and (3). In these expressions, N_c and M_{cz} are the design resistances of channel sections under pure compression and pure bending about the minor axis, respectively. The AISC design guide employs the same cross-section classification

limits as the European code EN 1993-1-4 [10], but adopts different approaches for the calculation of cross-sectional resistances (N_c and M_{cz}). For non-slender sections, N_c is equal to the yield load, while for slender sections, $N_c=Q_aQ_s\sigma_{0.2}A$ is calculated as the product of a reduced yield stress and the gross cross-section area, where Q_a and Q_s are reduction factors for slender stiffened (web) and unstiffened (flange) elements, respectively, determined according to Chapter 5 of AISC design guide 27 [11]. With regards to cross-sectional bending moment resistance, the AISC design guide uses the plastic moment capacity $M_{pl,z,Rd}$ but with a upper limit of $1.6M_{el,z,Rd}$ for compact channel sections (corresponding to Class 1 and 2 sections in EN 1993-1-4 [10]). In the determination of bending moment capacities for non-compact channel sections (corresponding to Class 3 sections in EN 1993-1-4 [10]), AISC design guide 27 [11] considers partial plasticity and thus yields higher predicted capacities than the elastic moment capacities calculated from the European code. However, for slender sections (corresponding to Class 4 sections in EN 1993-1-4), the adopted elastic critical buckling moment approach in the AISC design guide [11] generally leads to more conservative bending moment resistances than the EC3 effective moment capacities.

$$\frac{N_{Ed}}{N_c}+\frac{8}{9}\frac{M_{Ed,z}}{M_{cz}}\le 1, \quad \text{for } \frac{N_{Ed}}{N_c}\ge 0.2 \tag{2}$$

$$\frac{N_{Ed}}{2N_c}+\frac{M_{Ed,z}}{M_{cz}}\le 1, \quad \text{for } \frac{N_{Ed}}{N_c}< 0.2 \tag{3}$$

The accuracy of the provisions of AISC design guide 27 [11] is evaluated by comparing the combined loading test and numerical failure loads against the predicted strengths. The mean ratios of $N_u/N_{u,AISC}$ are equal to 2.29 and 1.72, with COV values of 0.24 and 0.11 for stainless steel channel sections under combined compression and minor axis bending moment in the ‘n’ and ‘u’ orientations, respectively. The AISC design guide was generally found to yield slightly more accurate and less scattered resistance predictions than EN 1993-1-4, owing

principally to the employment of a more efficient bi-linear design interaction curve [14]. The test results from the companion paper [9] are plotted against the EC3 and AISC design interaction curves in Figs 2 and 3, highlighting the scope for improvement in both sets of provisions.

4. Revised EC3 method

The current European code EN 1993-1-4 [10] employs a linear interaction formula for the design of Class 1 and 2 channel sections under combined compression and bending moment about the minor axis, without considering the favourable spread of plasticity within the cross-section, thus resulting in rather conservative and scattered resistance predictions. More efficient nonlinear design interaction formulae for channels are therefore sought herein, based on the assumption of fully plastic behaviour throughout the cross-section [21,22]; this assumption was successfully employed in the derivation of nonlinear design interaction formulae for Class 1 and 2 doubly-symmetric cross-sections (e.g., I-section and square, rectangular and circular hollow sections) subjected to combined loading. Fig. 4 illustrates the stress distribution for an I-section under combined compression and bending moment about the major axis, assuming full plasticity, where the inner compressive plastic stress block provides resistance to the applied compression force, but results in zero net bending moment about the design neutral axis (i.e. making no contribution to the cross-section bending resistance), while the outer pair of stress blocks lead to equal and opposite resultant forces (i.e. making no contribution to the cross-section compression resistance) and provide bending moment resistance; note that the design neutral axis is always located at the PNA for doubly symmetric cross-sections under combined loading, but this may not be the case for channel sections, as discussed later.

For channel sections under relatively low levels of axial compressive force and dominant minor axis bending moment, the plastic compressive stresses lie exclusively within the outstands, as shown in Fig. 5, where y_d is the distance from the design neutral axis to the outer face of the web, and a_1 and a_2 denote the heights of the compressive stress blocks below and above the design neutral axis, respectively. In this scenario, the design neutral axis is located at the PNA (i.e. y_d=y_p, where y_p is the distance from the PNA to the outer face of the web) and the plastic stress blocks associated with the axial compressive force are distributed symmetrically either side of the PNA (i.e. a_1=a_2=N_{Ed}/4$\sigma_{0.2}t_f$). The reduced cross-section plastic moment capacity $M_{N,z,Ed}$ is then given by Eq. (4). Note that Eq. (4) applies for channel sections under relatively low levels of axial compressive force with N_{Ed}<4$\sigma_{0.2}t_f$(y_p-t_w), where the plastic compressive stresses lie exclusively within the outstands.

$$M_{Ed} \le M_{N,z,Rd} = M_{pl,z,Rd} - \frac{N_{Ed}^2}{8\sigma_{0.2}t_f} \qquad \text{for } N_{Ed} < 4\sigma_{0.2}t_f\,(y_p - t_w) \quad (4)$$

For channel sections subjected to higher levels of axial compressive force and smaller bending moments, compressive stresses extend into the web (i.e. N_{Ed}≥4$\sigma_{0.2}t_f$(y_p-t_w)), as shown in Fig. 6. In this scenario, the location of the design neutral axis varies from the PNA to the ENA, as the applied compression force increases from the limit value N_{Ed}=4$\sigma_{0.2}t_f$(y_p-t_w) to the cross-section yield load N_{Ed}=$A\sigma_{0.2}$. Based on the assumption that the inner compressive plastic stress block results in zero net bending moment about the design neutral axis, with the resultant force equal to the applied compression load, and the outer pair of stress blocks lead to equal and opposite resultant forces, y_d, a_1 and a_2 can be determined, as given by Eqs (5) – (7). The reduced cross-section plastic moment capacity $M_{N,z,Ed}$ can then be calculated from Eq. (8).

$$y_d = \frac{1}{16N_{Ed}\sigma_{0.2}ht_f}(4b_f^2t_f^2h\sigma_{0.2}^2 - 8b_f^2t_f^3\sigma_{0.2}^2 - 4b_ft_ft_wh^2\sigma_{0.2}^2 + 16b_ft_f^3t_w\sigma_{0.2}^2 + t_w^2h^3\sigma_{0.2}^2 + 2t_ft_w^2h^2\sigma_{0.2}^2 - 4t_f^2t_w^2h\sigma_{0.2}^2 - 8t_f^3t_w^2\sigma_{0.2}^2 + 4N_{Ed}b_ft_fh\sigma_{0.2} + 8N_{Ed}b_ft_f^2\sigma_{0.2} - 2N_{Ed}t_wh^2\sigma_{0.2} + 8N_{Ed}t_ft_wh\sigma_{0.2} - 8N_{Ed}t_f^2t_w\sigma_{0.2} + N_{Ed}^2h - 2N_{Ed}^2t_f) \quad (5)$$

$$a_1 = \frac{1}{16N_{Ed}\sigma_{0.2}ht_f}(4b_f^2t_f^2h\sigma_{0.2}^2 - 8b_f^2t_f^3\sigma_{0.2}^2 - 4b_ft_ft_wh^2\sigma_{0.2}^2 + 16b_ft_f^3t_w\sigma_{0.2}^2 + t_w^2h^3\sigma_{0.2}^2 + 2t_ft_w^2h^2\sigma_{0.2}^2 - 4t_f^2t_w^2h\sigma_{0.2}^2 - 8t_f^3t_w^2\sigma_{0.2}^2 + 4N_{Ed}b_ft_fh\sigma_{0.2} - 8N_{Ed}b_ft_f^2\sigma_{0.2} - 2N_{Ed}t_wh^2\sigma_{0.2} + 8N_{Ed}t_f^2t_w\sigma_{0.2} + N_{Ed}^2h + 6N_{Ed}^2t_f) \quad (6)$$

$$a_2 = \frac{1}{16N_{Ed}\sigma_{0.2}ht_f}(-4b_f^2t_f^2h\sigma_{0.2}^2 + 8b_f^2t_f^3\sigma_{0.2}^2 + 4b_ft_ft_wh^2\sigma_{0.2}^2 - 16b_ft_f^3t_w\sigma_{0.2}^2 - t_w^2h^3\sigma_{0.2}^2 - 2t_ft_w^2h^2\sigma_{0.2}^2 + 4t_f^2t_w^2h\sigma_{0.2}^2 + 8t_f^3t_w^2\sigma_{0.2}^2 + 4N_{Ed}b_ft_fh\sigma_{0.2} - 8N_{Ed}b_ft_f^2\sigma_{0.2} - 2N_{Ed}t_wh^2\sigma_{0.2} + 8N_{Ed}t_f^2t_w\sigma_{0.2} + 3N_{Ed}^2h + 2N_{Ed}^2t_f) \quad (7)$$

$$M_{Ed} \le M_{N,z,Rd} = \frac{1}{16t_fh\sigma_{0.2}}(2b_ft_f\sigma_{0.2} - 2t_ft_w\sigma_{0.2} + t_wh\sigma_{0.2} - N_{Ed})(6b_ft_fh\sigma_{0.2} - 4b_ft_f^2\sigma_{0.2} - t_wh^2\sigma_{0.2} + 4t_f^2t_w\sigma_{0.2} + N_{Ed}h + 2N_{Ed}t_f) \quad (8)$$

Considering the rather lengthy nature of the analytical interaction expressions for channel sections subjected to combined compression and minor axis bending moment, simplified approximate interaction expressions that are more suitable for design calculations are sought. For this purpose, the general format of the interaction formulae given by Eq. (9) [23], which is often employed for representing cross-section resistances under combined compression and bending about the axis of symmetry, is considered, in which α_p is an exponent that can be chosen to fit the approximate expression to the full analytical results. Through comparisons of the approximate interaction curves, determined from Eq. (9) with a series of assumed α_p values, against the analytical interaction curves for a range of channel sections with different aspect ratios and sizes, it is concluded that α_p=2.0 be adopted, thus leading to Eq. (10) for Class 1 and 2 channel sections under combined compression and minor axis bending moment. Typical graphical comparisons between the analytical and approximate interaction curves for the two tested channel sections are shown in Figs 2 and 3, indicating excellent agreement.

Note that for Class 3 and Class 4 channel sections under minor axis combined loading, the linear design interaction formula, as given by Eq. (1), is still adopted.

$$\frac{M_{Ed}}{M_{pl,z,Rd}} = 1 - \left(\frac{N_{Ed}}{N_{pl,Rd}} \right)^{\alpha_p} \tag{9}$$

$$\frac{M_{Ed}}{M_{pl,z,Rd}} = 1 - \left(\frac{N_{Ed}}{N_{pl,Rd}} \right)^{2} \tag{10}$$

The accuracy of the revised EC3 method, utilising the proposed interaction nonlinear curve, is evaluated by comparing test (or FE) failure loads for Class 1 and 2 channel sections against the predicted failure loads. As shown in Table 3, the mean $N_u/N_{u,EC3,rev}$ ratios are equal to 1.34 and 1.46, with COV values of 0.07 and 0.06, for stainless steel Class 1 and 2 channel sections subjected to minor axis combined loading in the 'n' and 'u' orientations, respectively, revealing a higher level of design accuracy and consistency than the European code EN 1993-1-4 [10] and AISC design guide 27 [11]. The revised EC3 nonlinear design interaction curves, together with the EN 1993-1-4 and AISC design interaction curves, are plotted against the experimental results [9] in Figs 2 and 3, also showing the substantial improvement of the revised EC3 design method over the current design standards.

5. Continuous strength method (CSM)

5.1 General

The current cross-section design interaction curves for stainless steel channel sections subjected to minor axis combined loading given in both EN 1993-1-4 [10] and the AISC design guide [11] suffer from having an overly conservative shape and inaccurate end points.

The conservative shape does not adequately allow for the spread of plasticity within stainless steel channel sections under combined loading, while the compression and bending end points of the design interaction curves are determined based on the 0.2% proof stress as the failure stress without accounting for strain hardening. The revised EC3 nonlinear design interaction curve proposed in Section 4 takes into account the spread of plasticity within channel sections under combined loading, but is still anchored to the conservative EC3 end points (i.e. cross-section yield load and plastic moment capacity), thus leaving scope for further improvement. An improved design approach with more precise end points and the more efficient interaction curve from Section 4, anchored to these new end points, is developed and evaluated in this section.

The continuous strength method (CSM) [2–5] is a deformation-based design approach that allows account to be taken of strain hardening in the determination of cross-sectional compression and bending moment resistances. The CSM was originally developed for non-slender doubly symmetric cross-sections (e.g., tubular sections and I-sections) [2–4], and has been recently extended to cover the design of slender sections [5] and non-doubly symmetric cross-sections (e.g., mono-symmetric channel sections and T-sections, and asymmetric angle sections) [24]. Comparisons of test and FE results on stainless steel channel section stub columns and beams with the CSM capacity predictions generally indicated a high level of design accuracy and consistency [5,24]. Therefore, the CSM cross-sectional compression and bending moment resistances are ideal end points for the improved design interaction curves. A brief summary of the CSM for non-slender and slender channel sections under isolated loading cases is firstly described in Section 5.2; extension to cover combined loading cases is then presented in Section 5.3.

5.2 CSM for channel sections under isolated loading

The use of the CSM firstly requires determination of the deformation capacity (expressed as the maximum attainable compressive strain) of the cross-section under the applied loading; this is achieved by means of the CSM base curves, as given by Eqs (11) and (12) for non-slender [2] and slender [5] plated sections, respectively, where ε_{csm} is the maximum attainable compressive strain of the cross-section under the applied loading, ε_y is the yield strain, defined as $\sigma_{0.2}/E$, and $\bar{\lambda}_p = \sqrt{\sigma_{0.2}/\sigma_{cr}}$ is the cross-sectional slenderness, in which σ_{cr} is the cross-section elastic buckling stress under the applied loading, which may be calculated numerically (e.g., using the finite strip software CUFSM [25]) or from approximate analytical formulations [26]. Note that $\bar{\lambda}_p = 0.68$ defines the boundary between non-slender and slender plated sections, at which point the maximum attainable compressive strain is equal to the yield strain (i.e. $\varepsilon_{csm}/\varepsilon_y$=1).

$$\frac{\varepsilon_{csm}}{\varepsilon_y} = \frac{0.25}{\bar{\lambda}_p^{3.6}} \text{ but } \leq \min\left(15, \frac{C_1\varepsilon_u}{\varepsilon_y}\right), \quad \text{for } \bar{\lambda}_p \leq 0.68 \tag{11}$$

$$\frac{\varepsilon_{csm}}{\varepsilon_y} = \left(1 - \frac{0.222}{\bar{\lambda}_p^{1.050}}\right)\frac{1}{\bar{\lambda}_p^{1.050}}, \quad \text{for } \bar{\lambda}_p > 0.68 \tag{12}$$

Upon calculation of the limiting (failure) strain, the CSM bi-linear (elastic, linear hardening) material model is utilised for the determination of cross-section resistance, allowing design stresses greater than the yield (0.2% proof) stress to be achieved. The CSM bi-linear material model is depicted in Fig. 7, where C_1, C_2, C_3 and C_4 are the CSM material coefficients, of which the values were calibrated based on material tensile coupon test data [27]. Note that a quad-linear material model suitable for representing the stress-strain response of hot-rolled steel, including the characteristic yield plateau, has also been developed [28]. The material

coefficient C_1 is utilised to define a cut-off strain in the CSM base curve for non-slender plated sections (see Eq. (11)), to avoid over-predicting failure strengths from the adopted CSM material model. The coefficient C_2, as adopted in Eq. (13), defines the material strain hardening slope E_{sh}, while C_3 and C_4 are used to predict the strain at the ultimate strength of the material $\varepsilon_u=C_3(1-\sigma_{0.2}/\sigma_u)+C_4$. For austenitic stainless steel, values of C_1, C_2, C_3 and C_4 are equal to 0.1, 0.16, 1.0 and 0.0, respectively [27].

$$E_{sh} = \frac{\sigma_u - \sigma_{0.2}}{C_2\varepsilon_u - \varepsilon_y} \tag{13}$$

The CSM design stress σ_{csm} is then determined from Eq. (14); for non-slender sections with strain ratios $\varepsilon_{csm}/\varepsilon_y$ greater than unity, the design stress σ_{csm}, derived from the CSM elastic, strain hardening material model, exceeds the yield (0.2% proof) stress, which is the design stress used in the current international design standards, while for slender cross-section, $\sigma_{csm}<\sigma_{0.2}$ reflects the earlier onset of local buckling. The CSM cross-section compression resistance $N_{csm,Rd}$ is directly calculated as the product of the design stress σ_{csm} and the gross cross-section area A, as given by Eq. (15), where γ_{M0} is a partial factor for cross-section resistance, with a recommended value of 1.1 for stainless steel.

$$\begin{aligned} \sigma_{csm} &= E\varepsilon_{csm} && \text{for } \varepsilon_{csm} < \varepsilon_y \\ \sigma_{csm} &= \sigma_{0.2} + E_{sh}\left(\varepsilon_{csm} - \varepsilon_y\right) && \text{for } \varepsilon_{csm} \geq \varepsilon_y \end{aligned} \tag{14}$$

$$N_{csm,Rd} = \frac{A\sigma_{csm}}{\gamma_{M0}} \tag{15}$$

For channel sections under minor axis bending, the neutral axis is not located at the centreline of the cross-section, and thus the maximum outer-fibre compressive and tensile strains are not equal. In this case, the CSM limiting compressive strain $\varepsilon_{csm,c}$ is determined from the CSM base curves given by Eqs (11) and (12), while the corresponding outer-fibre tensile strain

$\varepsilon_{csm,t}$ is obtained based on the assumption of a linearly-varying through-depth strain distribution, as given by Eq. (16), where b_f is the outer flange width and y_c is the distance from the design neutral axis to the outer compressive fibre (see Figs 8(a) and 8(b)).

$$\varepsilon_{csm,t} = \frac{\varepsilon_{csm,c}\left(b_f - y_c\right)}{y_c} \tag{16}$$

Theofanous et al. [29] and Zhao and Gardner [24] carried out experimental and numerical studies to investigate the evolution of the neutral axis position of stainless steel angle and channel sections in bending, and found that for non-slender sections, the neutral axis position at failure is located between the elastic and plastic neutral axes (approximately at the mid-point of the two), while for more slender sections, the neutral axis positon at failure remains close to the elastic neutral axis. Therefore, the CSM design neutral axis is assumed to be located at the mid-point between the elastic and plastic neutral axes for channel sections with $\bar{\lambda}_p \leq 0.6$, and located at the elastic neutral axis for relatively slender sections with $\bar{\lambda}_p > 0.6$ [24].

Upon identification of the tensile and compressive limiting strains ($\varepsilon_{csm,c}$ and $\varepsilon_{csm,t}$), the design stress distribution can then be determined from the adopted CSM bi-linear (elastic, linear hardening) material model. If the maximum design strain $\varepsilon_{csm,max}$, taken as the maximum of $\varepsilon_{csm,c}$ and $\varepsilon_{csm,t}$, is less than the yield strain ε_y, the resulting design stress distribution is elastic and linear-varying, with no benefit arising from strain hardening, and the CSM cross-section bending resistance $M_{csm,Rd}$ is thus directly calculated as the elastic moment capacity multiplied by the strain ratio, as given by Eq. (17), with $\varepsilon_{csm}=\varepsilon_{csm,max}$. If the maximum design strain $\varepsilon_{csm,max}$ is greater than the yield strain ε_y, indicating that at least one of the tensile and compressive portions of the channel section benefits from strain hardening, $M_{csm,Rd}$ is

determined from Eq. (18), in which α is the CSM bending coefficient [3]. Derivation of the α coefficients for channel sections, as well as other mono-symmetric T-sections and asymmetric angle sections in bending about both geometric axes, is described in Zhao and Gardner [24], with the recommended values reported herein in Table 4.

$$M_{csm,Rd} = \frac{\varepsilon_{csm}}{\varepsilon_y}\frac{W_{el}\sigma_{0.2}}{\gamma_{M0}} \qquad \text{for } \varepsilon_{csm} < \varepsilon_y \tag{17}$$

$$M_{csm,Rd} = \frac{W_{pl}\sigma_{0.2}}{\gamma_{M0}}\left[1+\frac{E_{sh}}{E}\frac{W_{el}}{W_{pl}}\left(\frac{\varepsilon_{csm}}{\varepsilon_y}-1\right)-\left(1-\frac{W_{el}}{W_{pl}}\right)/\left(\frac{\varepsilon_{csm}}{\varepsilon_y}\right)^{\alpha}\right] \quad \text{for } \varepsilon_{csm} \geq \varepsilon_y \tag{18}$$

Note that for slender channel sections (i.e. $\bar{\lambda}_p > 0.68$) under minor axis bending in the 'n' orientation, where the design neutral axis is closer to the compressive outer fibre, although the limiting compressive strain $\varepsilon_{csm,c}$ is less than the yield strain ε_y, the corresponding maximum tensile strain $\varepsilon_{csm,t}$ can be significantly larger than the yield strain. Benefit therefore arises from both the spread of plasticity and strain hardening, enabling ultimate bending moment resistances that can be even greater than the plastic moment capacity. This behaviour, which is predicted by the CSM [5,24] and observed in physical tests [29], is in contrast to the effective moment capacity determined from EN 1993-1-4 [10], as illustrated in Fig. 9, where the EC3 and CSM design strain and stress distributions for a slender channel section in bending about the minor axis in the 'n' orientation are shown. The strains corresponding to the EC3 design approach are denoted $\varepsilon_{EC3,c}$ and $\varepsilon_{EC3,t}$ at the compressive and tensile fibres, while the corresponding stresses are denoted $\sigma_{EC3,c}$ and $\sigma_{EC3,t}$.

5.3 CSM for channel sections under combined loading

The ultimate loads and moments obtained from the experimental programme conducted in the companion paper [9], together with the numerical results derived from the parametric studies performed in the present paper, have been normalised by the CSM cross-section compression and bending moment resistances, and plotted in Figs 10(a) and 10(b). The normalised data points may be seen to follow a much tighter trend in comparison to those normalised by the cross-section yield load and plastic bending moment resistance in Figs 1(a) and 1(b). This indicates that the use of the CSM cross-section compression and bending moment capacities as the end points of the design interaction curves can substantially reduce the conservatism and scatter of the predictions. The next step is to consider the shape of the interaction curve for stainless steel channel sections subjected to the combined actions of compression and minor axis bending moment to be anchored to these more precise CSM end points.

Based on the findings of Section 4 and considering the general distribution of the normalised test and numerical data points in Figs 10(a) and 10(b), it is proposed to adopt an interaction curve of the nonlinear form defined by Eq. (10), but with the CSM cross-sectional capacities as the end points, for stocky channel sections under combined compression and minor axis bending moment. The proposed CSM nonlinear interaction formula is thus given by Eq. (19) for channel sections with $\bar{\lambda}_p \leq 0.6$, in which $M_{csm,z,Rd}$ is the CSM cross-sectional resistance in bending about the minor axis, as calculated from Eq. (18), with the design neutral axis assumed to be located at the mid-point between the ENA and PNA, and $M_{Ed,z}=N_{Ed}(e_0+e')$ is the design applied bending moment about the minor axis, where e_0 is the initial loading eccentricity taken equal to the distance from the initial loading point to the mid-point between the ENA and PNA (i.e. the CSM design neutral axis at failure). The proposed CSM nonlinear

design interaction curves are also plotted in Figs 10(a) and 10(b), revealing an excellent representation of the distribution of the experimental and numerical data points. For channel sections with $\bar{\lambda}_p > 0.6$, the corresponding cross-section interaction behaviour becomes increasingly linear, and a linear design interaction curve is thus adopted, as given by Eq. (20), where both the design applied bending moment $M_{Ed,z}=N_{Ed}(e_0+e')$ and the CSM cross-sectional bending moment resistance $M_{csm,z,Rd}$ are calculated based on the design neutral axis located at the ENA.

$$\frac{M_{Ed}}{M_{csm,z,Rd}} = 1 - \left(\frac{N_{Ed}}{N_{csm,Rd}} \right)^2 \qquad \text{for } \bar{\lambda}_p \le 0.60 \qquad (19)$$

$$\frac{N_{Ed}}{N_{csm,Rd}} + \frac{M_{Ed}}{M_{csm,z,Rd}} \le 1 \qquad \text{for } \bar{\lambda}_p > 0.60 \qquad (20)$$

The CSM design proposals are evaluated by comparing the experimental and numerical failure loads against the corresponding resistance predictions. The mean ratios of $N_u/N_{u,csm}$, as shown in Tables 2(a) and 2(b), are equal to 1.21 and 1.19, with COVs of 0.05 and 0.05, for stainless steel channel sections subjected to combined compression and minor axis bending moment in the ‘n’ and ‘u’ orientations, respectively. Compared to the European code EN 1993-1-4 [10] and AISC design guide 27 [11], the new CSM proposals may be seen to substantially improve the design accuracy by around 90%, and reduce the scatter of the capacity predictions by about 70%; the higher level of accuracy and consistency of the CSM design proposals is also evident in Figs 11 and 12, where the resistances determined from the CSM and the current design standards (EN 1993-1-4 [10] and AISC [11]) are plotted against the experimentally and numerically derived failure loads.

6. Summary

Summing up of the findings of Sections 3, 4 and 5, the European code EN 1993-1-4 [10] was found to yield the most conservative and scattered resistance predictions for stainless steel channel sections subjected to combined compression and minor axis bending moment, owing to the adoption of a linear design interaction curve and the employment of conservative compression and bending end points without accounting for strain hardening. The AISC design guide 27 [11] provides more accurate and consistent resistance predictions than EN 1993-1-4 [10], principally due to the use of a bi-linear design interaction curve. Revised nonlinear design interaction curves were proposed for Class 1 and 2 channel sections under minor axis combined loading in Section 4, based on the assumption of full plasticity throughout the cross-section; this revised EC3 method was shown to provide a higher level of design accuracy and consistency than the two design codes. The CSM has been extended to cover the design of channel sections under combined compression and minor axis bending, and shown to substantially improve the design accuracy and consistency over the current design standards, owing to the use of more efficient design interaction curves and the consideration of strain hardening in the determination of the compression and bending end points.

The four design approaches may also be evaluated based on the experimental results only. The mean ratios of the test failure loads to the predicted failure loads from the aforementioned design methods $N_{u,test}/N_{u,pred}$ are presented in Table 5, indicating that both of the proposed CSM and revised EC3 design approach yield a much higher level of design accuracy and consistency in predicting the resistance of stainless steel channel sections under combined compression and minor axis bending moment in comparison to current provisions.

7. Reliability analysis

Statistical analyses are performed herein to evaluate the reliability of the proposed CSM and revised EC3 design approach, based on a total of 654 test and numerical results and according to the EN 1990 requirements [30]. In the present reliability analysis, the material over-strength ratio for austenitic stainless steel and the corresponding COV were respectively taken as 1.3 and 0.06, and the COV of the geometric properties of stainless steel cross-sections was equal to 0.05, following the recommendations of Afshan et al. [31]. Table 6 reports the key obtained statistical parameters for both design proposals, in which $k_{d,n}$ is the design fractile factor (ultimate limit state), b is the mean ratio of test and numerical resistances to design model resistances, V_δ is the COV of the test and numerical simulation capacities relative to the resistance model, V_r is the combined COV incorporating both model and basic variable uncertainties, and γ_{M0} is the partial safety factor for stainless steel cross-section resistance. The resulting (required) partial factors for both design proposals, as reported in Table 6, are less than 1.1, which is the value recommended in EN 1993-1-4 [10], therefore demonstrating the reliability of the two proposed design approaches.

8. Conclusions

The numerical simulation and design of stainless steel channel sections under combined compression and minor axis bending have been the focus of the present paper. Using the numerical models validated in the companion paper [9], parametric studies were conducted to generate additional structural performance data over a wider range of cross-section aspect ratios and slendernesses, loading combinations and bending orientations. The numerical results generated in the present paper and the test data obtained from the companion paper [9]

were then employed to evaluate the accuracy of the existing design provisions for stainless steel channel sections under combined compression and minor axis bending moment, as given in the European code EN 1993-1-4 [10] and AISC design guide 27 [11], revealing rather conservative and scattered strength predictions; this can be attributed to the adoption of inaccurate design interaction curves and the employment of conservative cross-section compression and bending resistances as the end points that are determined without accounting for strain hardening. Revised nonlinear design interaction curves were then proposed for Class 1 and 2 channel sections under minor axis combined loading, assuming full plasticity throughout the cross-section, which were found to offer more accurate and consistent strength predictions than the current design standards. The deformation-based continuous strength method (CSM) was also extended to cover the design of stainless steel channel sections under the combined actions of compression and minor axis bending moment; the new CSM proposals adopt the derived plastic interaction curves but anchored to the CSM end points to allow for strain hardening; following comparisons with the test and numerical data, the new CSM proposals were shown to yield a substantially higher level of design accuracy and consistency than the European code EN 1993-1-4 [10] and AISC design guide 27 [11]. Finally, statistical analyses were performed to confirm the reliability of the proposed CSM and revised EC3 design approach, according to the EN 1990 requirements [30].

References

[1] Zhao O, Gardner L, Young B. Behaviour and design of stainless steel SHS and RHS beam-columns. Thin-Walled Structures, 2016;106:330–45.

[2] Afshan S, Gardner L. The continuous strength method for structural stainless steel design. Thin-Walled Structures, 2013;68(4):42–9.

[3] Gardner L, Wang F, Liew A. Influence of strain hardening on the behavior and design of steel structures. International Journal of Structural Stability and Dynamics, 2011;11(05):855–75.

[4] Liew A, Gardner L. Ultimate capacity of structural steel cross-sections under compression, bending and combined loading. Structures, 2015;1:2–11.

[5] Zhao O, Afshan S, Gardner L. Structural response and continuous strength method design of slender stainless steel cross-sections. Engineering Structures, 2017;140:14–25.

[6] Becque J, Lecce M, Rasmussen KJR. The direct strength method for stainless steel compression members. Journal of Constructional Steel Research, 2008;64(11):1231–8.

[7] Schafer BW. Review: The direct strength method of cold-formed steel member design. Journal of Constructional Steel Research, 2008;64(7):766–78.

[8] Huang Y, Young B. Experimental and numerical investigation of cold-formed lean duplex stainless steel flexural members. Thin-Walled Structures, 2013;73:216–28.

[9] Liang Y, Zhao O, Long Y, Gardner L. Laser-welded stainless steel channel sections under combined compression and minor axis bending – Part 1: Experimental study and numerical modelling. Journal of Constructional Steel Research, submitted.

[10] EN 1993-1-4:2006+A1:2015. Eurocode 3: Design of steel structures – Part 1.4: General rules – Supplementary rules for stainless steels, including amendment A1 (2015). Brussels: European Committee for Standardization (CEN); 2015.

[11] AISC. Design Guide 27: Structural Stainless Steel. American Institute of Steel Construction (AISC); 2013.

[12] Dawson RG, Walker AC. Post-buckling of geometrically imperfect plates. Journal of the Structural Division (ASCE), 1972;98(1):75–94.

[13] Gardner L, Nethercot DA. Numerical modeling of stainless steel structural components – A consistent approach. Journal of Structural Engineering (ASCE), 2004;130(10):1586–601.

[14] Liang, Y, Wang, F, Zhao, O, Long, Y, Gardner, L. Cross-section resistance of stainless steel channel sections subjected to combined axial compression and major axis bending. Journal of Constructional Steel Research, submitted.

[15] Zhao O, Rossi B, Gardner L, Young B. Experimental and numerical studies of ferritic stainless steel tubular cross-sections under combined compression and bending. Journal of Structural Engineering (ASCE), 2016;142(2):04015110.

[16] Zhao O, Gardner L, Young B. Buckling of ferritic stainless steel members under combined axial compression and bending. Journal of Constructional Steel Research, 2016;117:35–48.

[17] Zhao O, Gardner L, Young B. Experimental Study of Ferritic Stainless Steel Tubular Beam-Column Members Subjected to Unequal End Moments. Journal of Structural Engineering (ASCE), 2016; 142(11):04016091.

[18] Zhao O, Rossi B, Gardner L, Young B. Behaviour of structural stainless steel cross-sections under combined loading – Part II: Numerical modelling and design approach. Engineering Structures, 2015;89:247–59.

[19] EN 1993-1-1. Eurocode 3: Design of steel structures – Part 1.1: General rules and rules for buildings. Brussels: European Committee for Standardization (CEN); 2005.

[20] Zhao O, Gardner L, Young B. Structural performance of stainless steel circular hollow sections under combined axial load and bending – Part 2: Parametric studies and design. Thin-Walled Structures, 2016;101:240–8.

[21] Lindner J. Design of beams and beam columns. Progress in Structural Engineering and Materials, 2003;5(1):38–47.

[22] Boissonnade N, Greiner R, Jaspart JP, Lindner J. Rules for Member Stability in EN 1993-1-1: Background documentation and design guidelines. ECCS European Convention for Constructional Steelwork, 2006.

[23] da Silva LS, Simões R, Gervásio H. Design of Steel Structures: Eurocode 3: Design of Steel Structures, Part 1-1: General Rules and Rules for Buildings. John Wiley & Sons, 2016.

[24] Zhao O, Gardner L. Design of non-doubly symmetric stainless steel sections in bending. Journal of Constructional Steel Research, submitted.

[25] Schafer BW, Ádány S. Buckling analysis of cold-formed steel members using CUFSM: conventional and constrained finite strip methods. Proceedings of the Eighteenth International Speciality Conference on Cold-formed Steel Structures, Orlando, USA; 2006.

[26] Seif M, Schafer BW. Local buckling of structural steel shapes. Journal of Constructional Steel Research, 2010;66(10):1232–47.

[27] Buchanan C, Gardner L, Liew A. The continuous strength method for the design of circular hollow sections. Journal of Constructional Steel Research, 2016;118:207–16.

[28] Yun X, Gardner L. Stress-strain curves for hot-rolled steels. Journal of Constructional Steel Research, 2017;133:36–46.

[29] Theofanous M, Liew A, Gardner L. Experimental study of stainless steel angles and channels in bending. Structures, 2015;4:80–90.

[30] EN 1990. Eurocode – basis of structural design. Brussels: European Committee for Standardization (CEN); 2002.

[31] Afshan S, Francis P, Baddoo NR, Gardner L. Reliability analysis of structural stainless steel design provisions. Journal of Constructional Steel Research, 2015;114:293–304.

Table 1 Summary of modelled eccentrically loaded channel sections in the parametric studies.

Cross-section type	Orientation	h	b	t_w/t_f	e_{0e}	No. of FE models
Channel section	n	100 mm	Ranging from 33 mm to 100 mm	Ranging from 3 mm to 12.5 mm	Ranging from 1.8 mm to 654 mm	320
	u	100 mm	Ranging from 33 mm to 100 mm	Ranging from 3 mm to 12.5 mm	Ranging from 1.8 mm to 654 mm	320

Table 2 Comparisons of stainless steel channel section combined loading test and FE results with predicted resistances.

(a) In the 'n' orientation

No. of tests: 10 No. of FE simulations: 320	$N_u/N_{u,EC3}$	$N_u/N_{u,AISC}$	$N_u/N_{u,csm}$
Mean	2.31	2.29	1.21
COV	0.27	0.24	0.05

(a) In the 'u' orientation

No. of tests: 4 No. of FE simulations: 320	$N_u/N_{u,EC3}$	$N_u/N_{u,AISC}$	$N_u/N_{u,csm}$
Mean	1.85	1.72	1.19
COV	0.14	0.11	0.05

Table 3 Comparisons of stainless steel Class 1 and 2 channel section combined loading test and FE results with predicted resistances.

(a) In the 'n' orientation

No. of tests: 10 No. of FE simulations: 123	$N_u/N_{u,EC3}$	$N_u/N_{u,AISC}$	$N_u/N_{u,EC3,rev}$	$N_u/N_{u,csm}$
Mean	1.61	1.76	1.34	1.24
COV	0.07	0.17	0.07	0.05

(b) In the 'u' orientation

No. of tests: 4 No. of FE simulations: 138	$N_u/N_{u,EC3}$	$N_u/N_{u,AISC}$	$N_u/N_{u,EC3,rev}$	$N_u/N_{u,csm}$
Mean	1.80	1.72	1.46	1.19
COV	0.10	0.09	0.06	0.05

Table 4 Summary of values of CSM bending coefficient α.

Cross-section type	Axis of bending	Aspect ratio	α
Channel section	y-y	Any	2.0
	z-z	$h/b \leq 2$	1.5
		$h/b > 2$	1.0
T-section	y-y	$h/b < 1$	1.0
		$h/b \geq 1$	1.5
	z-z	Any	1.2
Angle	y-y	Any	1.5
	z-z	Any	1.0
SHS/RHS	Any	Any	2.0
CHS	Any	–	2.0
I-section	y-y	Any	2.0
	z-z	Any	1.2

Table 5 Comparisons of stainless steel channel section combined loading test results with predicted resistances.

No. of tests: 14	$N_{u,test}/N_{u,EC3}$	$N_{u,test}/N_{u,AISC}$	$N_{u,test}/N_{u,EC3,rev}$	$N_{u,test}/N_{u,csm}$
Mean	1.58	1.56	1.28	1.12
COV	0.08	0.07	0.08	0.06

Table 6 Summary of statistical evaluation of resistance predictions determined from the proposed CSM and revised EC3 approach.

Method	No. of tests and FE data	$k_{d,n}$	b	V_δ	V_r	γ_{M0}
CSM	654	3.105	1.209	0.054	0.095	0.85
Revised EC3	275	3.126	1.486	0.093	0.122	0.76

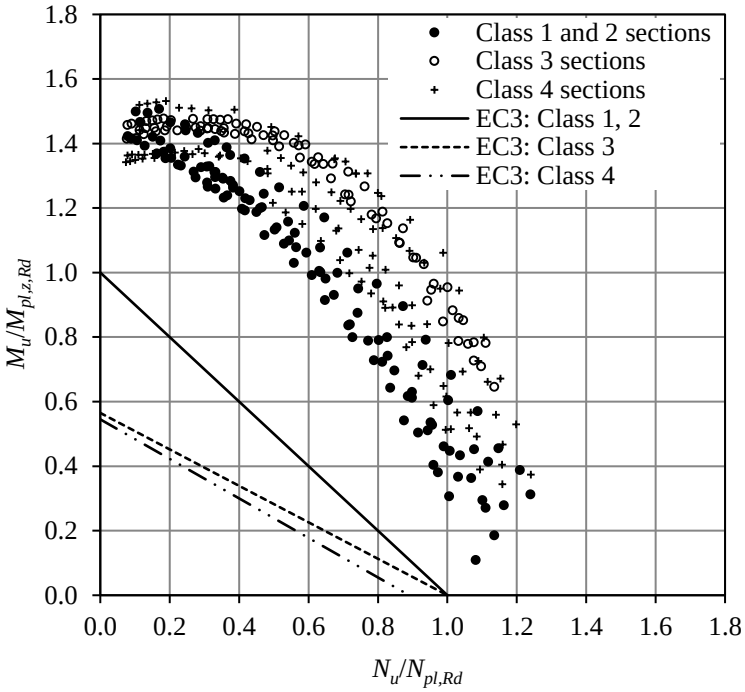

(a) In the 'n' orientation

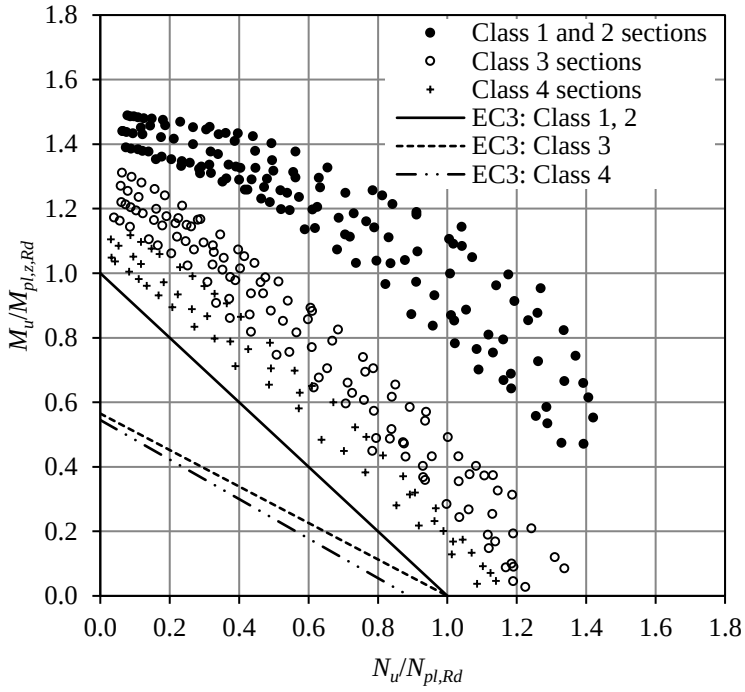

(b) In the 'u' orientation

Fig. 1. Combined loading test and FE results normalised by the plastic moment capacity and yield load.

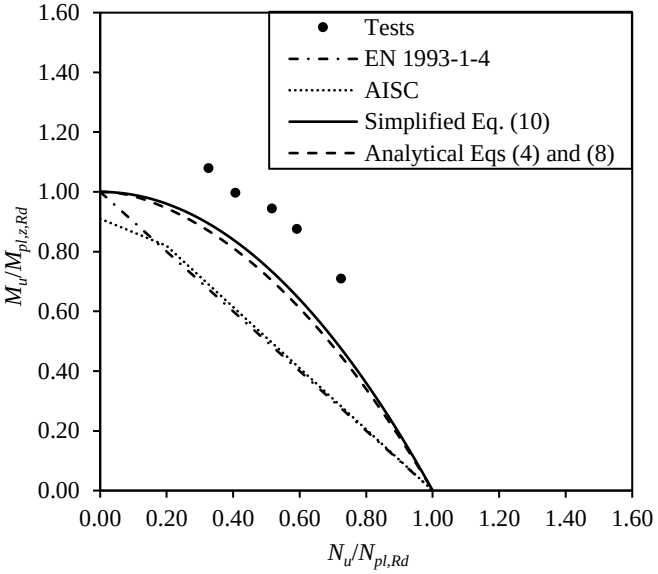

(a) C 100×50×6×9 specimens.

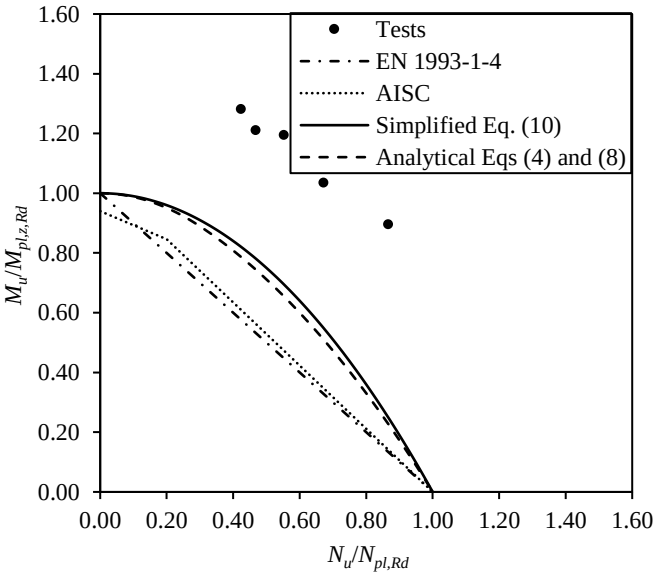

(b) C 40×40×5×5 specimens.

Fig. 2. Comparison of 'n' orientation combined loading test results with considered design interaction curves.

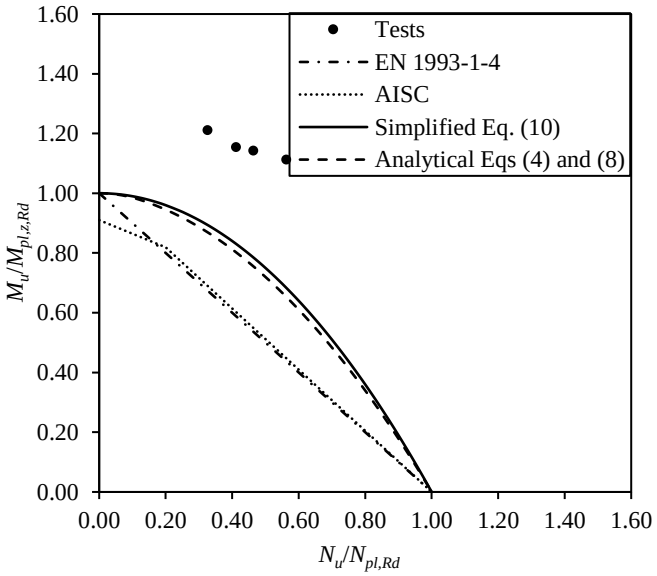

Fig. 3. Comparison of 'u' orientation combined loading test results on C 100×50×6×9 specimens with considered design interaction curves.

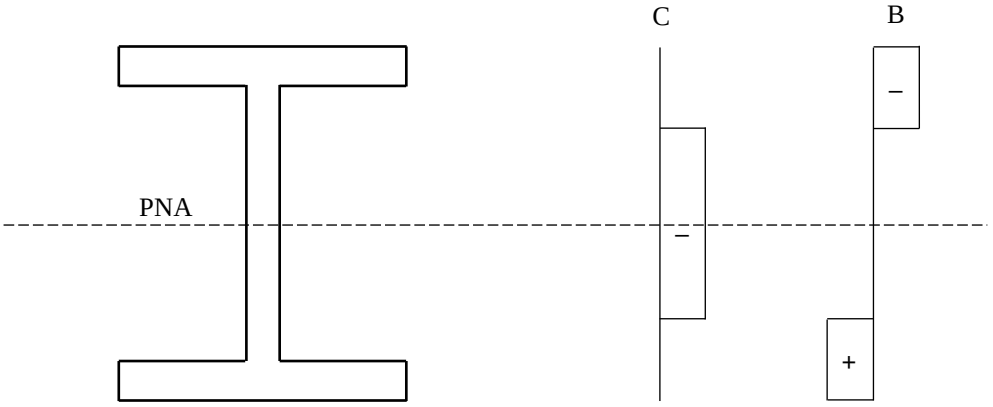

Fig. 4. Stress distribution for I-sections under major axis combined loading, assuming full plasticity. Note that '–' and '+' indicate compressive and tensile stresses, respectively, and 'C' and 'B' identify stress blocks for compression and bending resistances, respectively.

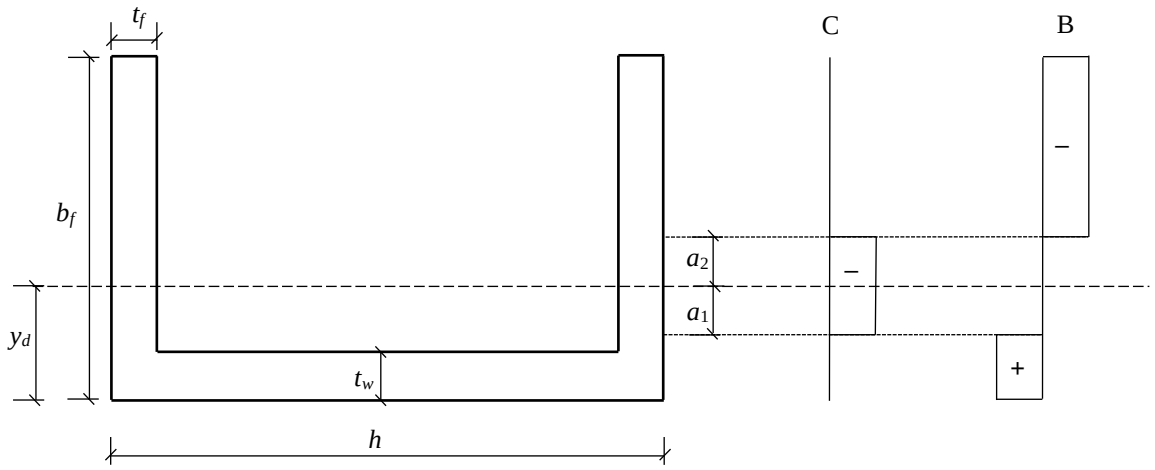

Fig. 5. Stress distribution for channel sections under minor axis combined loading, assuming full plasticity, where the stress block associated with the axial compressive load does not extend into the web. Note that '–' and '+' indicate compressive and tensile stresses, respectively, and 'C' and 'B' identify stress blocks for compression and bending resistances, respectively.

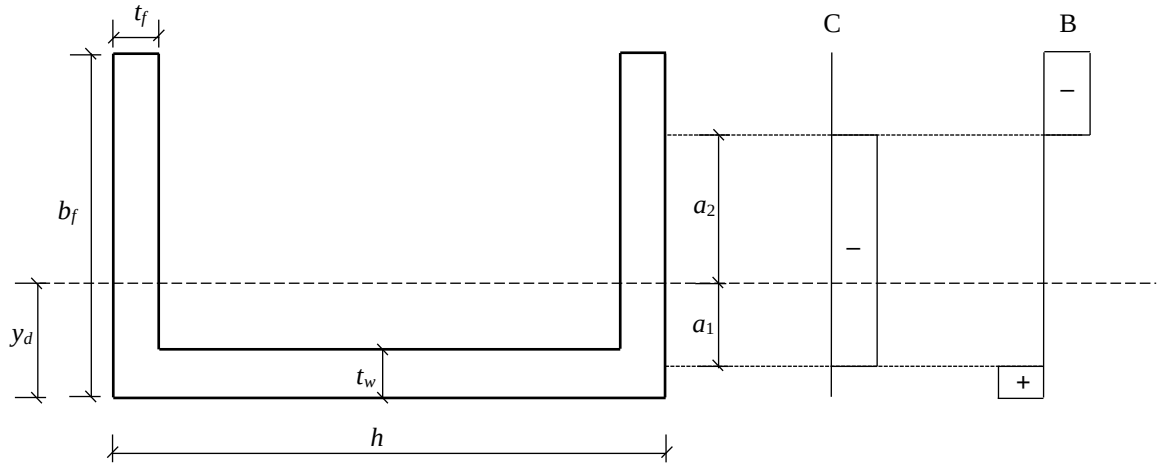

Fig. 6. Stress distribution for channel sections under minor axis combined loading, assuming full plasticity, where the stress block associated with the axial compressive load extends into the web. Note that '–' and '+' indicate compressive and tensile stresses, respectively, and 'C' and 'B' identify stress blocks for compression and bending resistances, respectively.

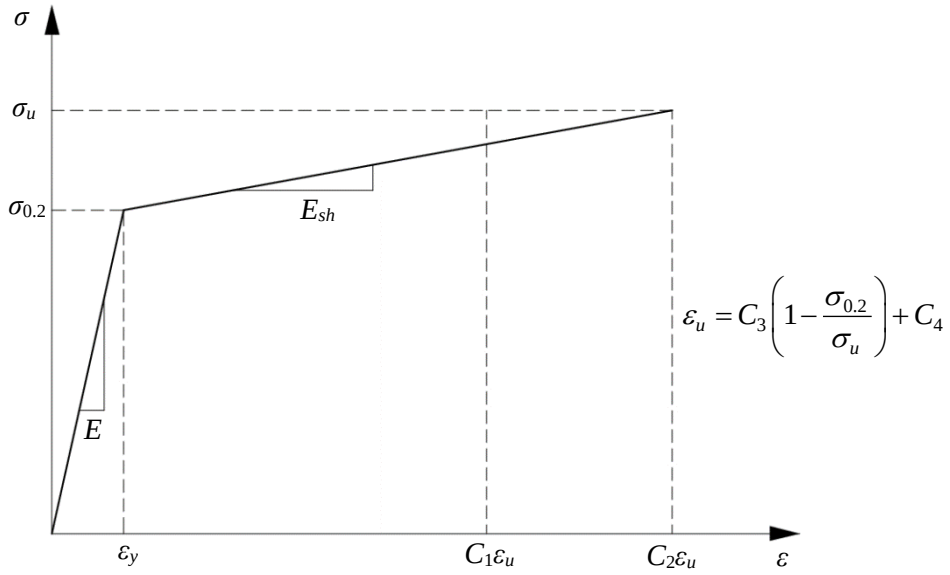

Fig. 7. CSM elastic, linear hardening material model.

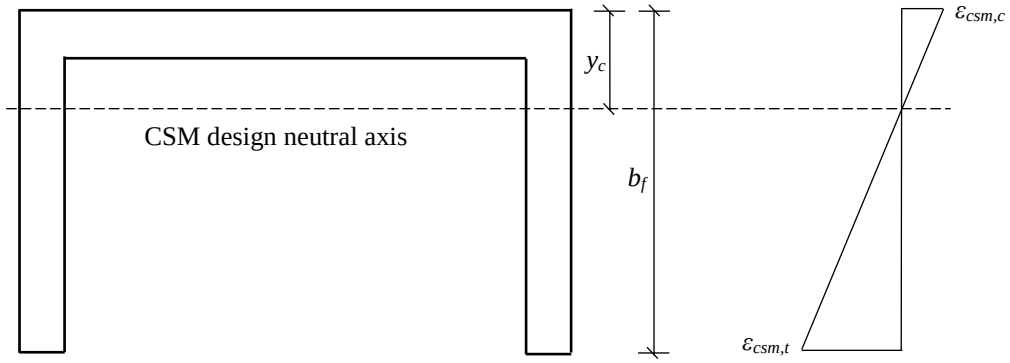

(a) In the ‘n’ orientation

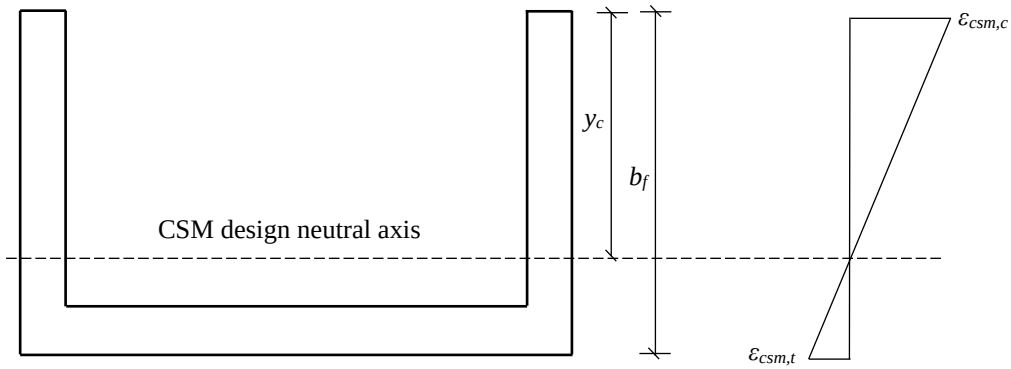

(b) In the ‘u’ orientation

Fig. 8. Definition of y_c and b_f for channels in bending in the ‘n’ and ‘u’ orientations.

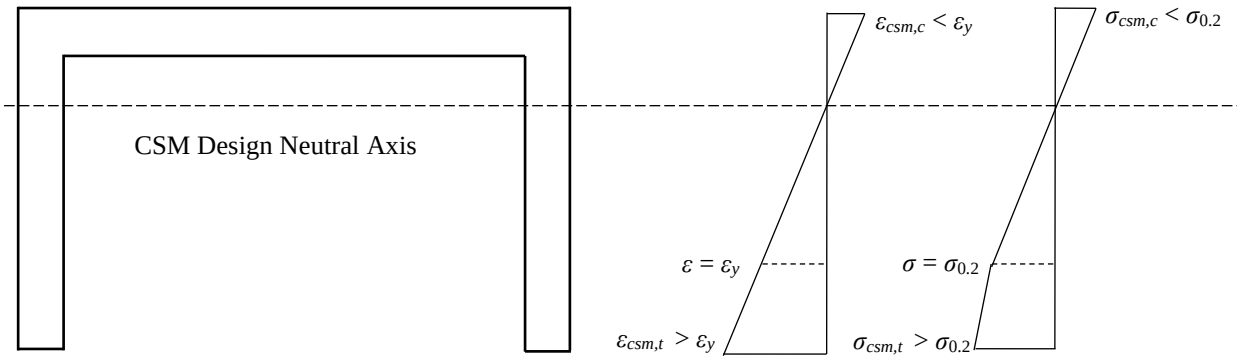

(a) CSM

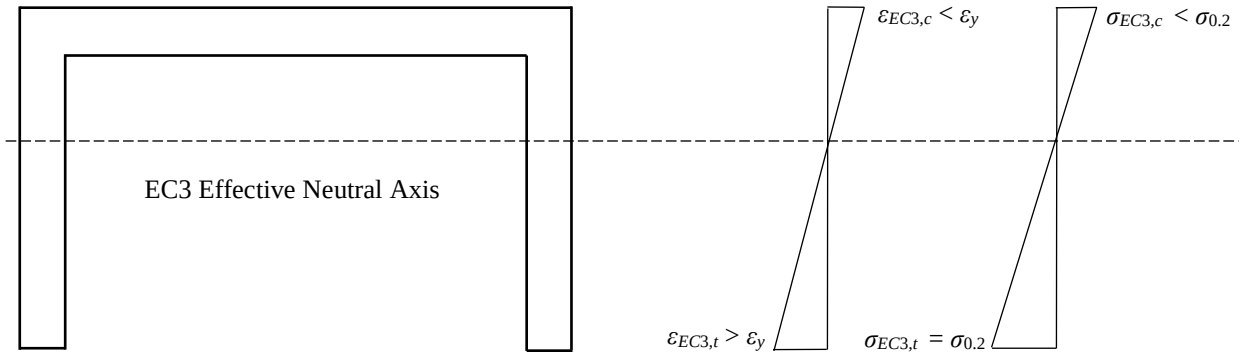

(b) EN 1993-1-4

Fig. 9. Comparison of EN 1993-1-4 and CSM design strain and stress distributions for slender channel sections under minor axis bending in the ‘n’ orientation.

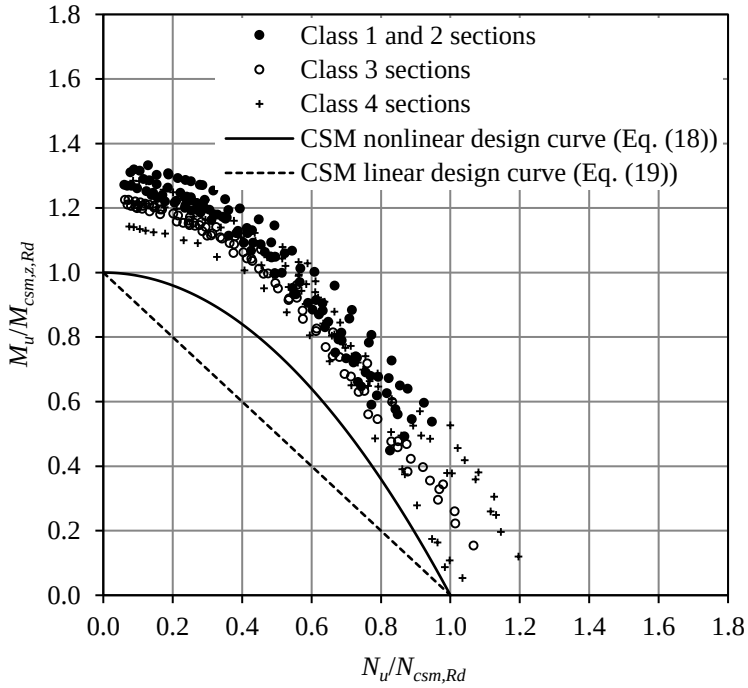

(a) In the 'n' orientation

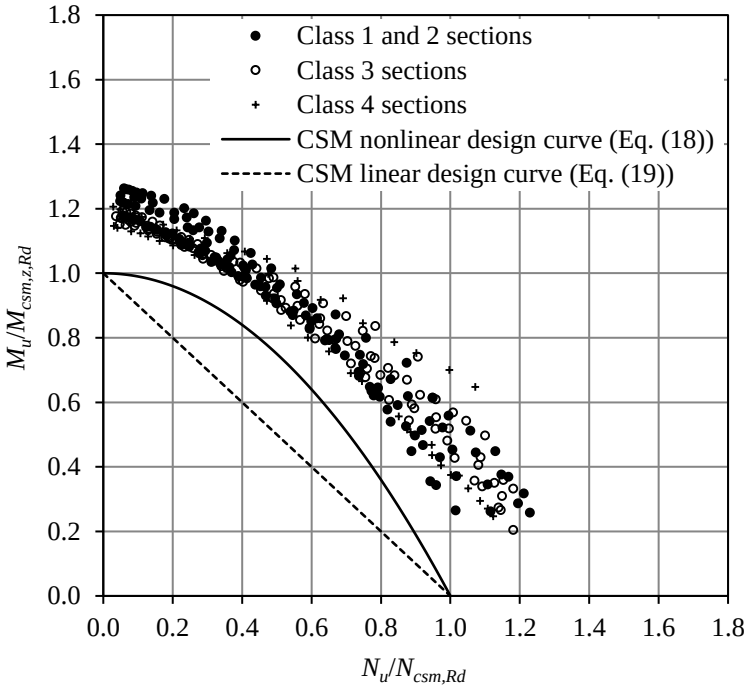

(b) In the 'u' orientation

Fig. 10. Combined loading test and FE results normalised by the CSM compression and bending resistances.

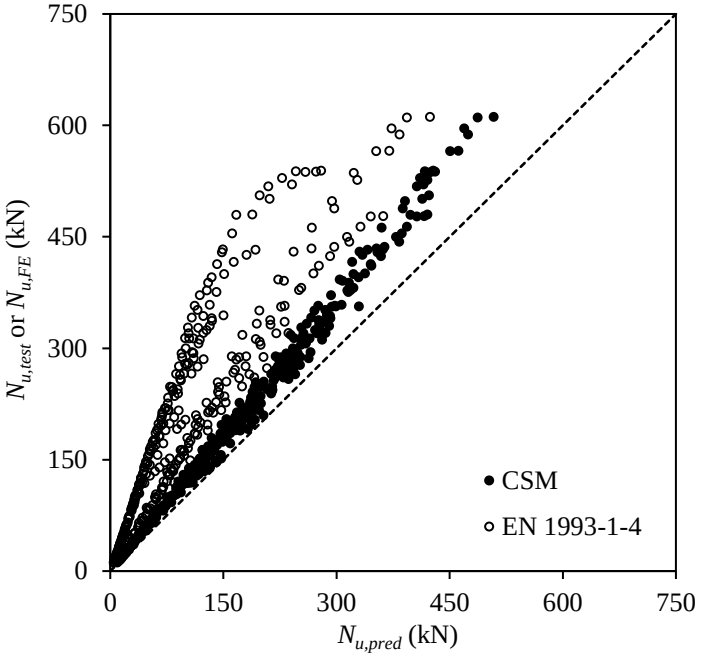

(a) In the 'n' orientation

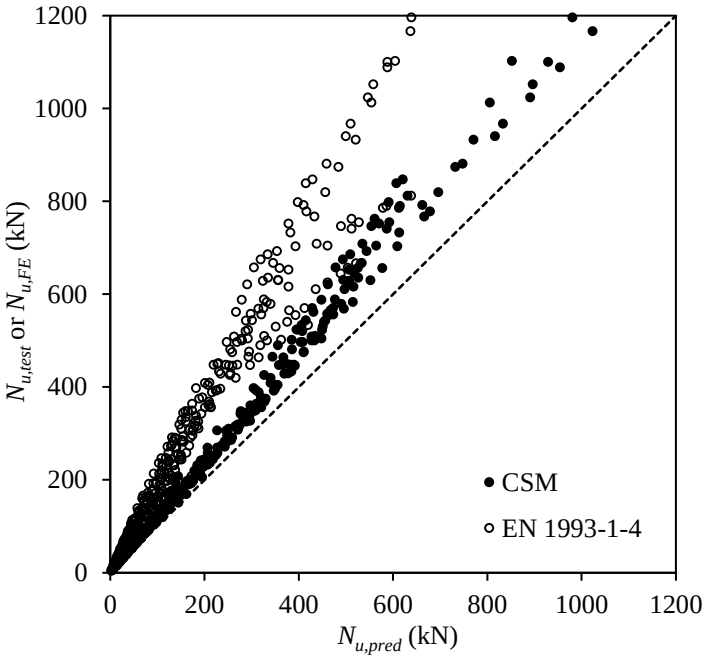

(b) In the 'u' orientation

Fig. 11. Comparison of combined loading test and FE results with CSM and EN 1993-1-4 capacity predictions.

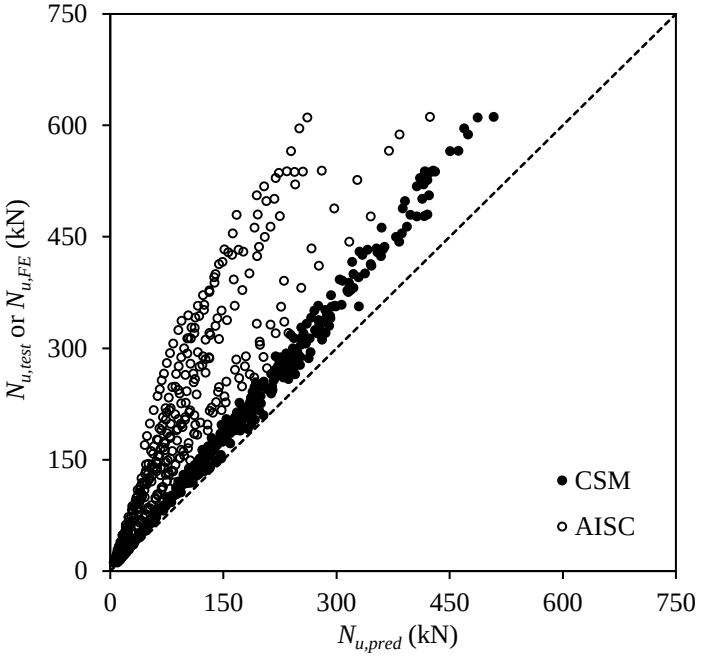

(a) In the 'n' orientation

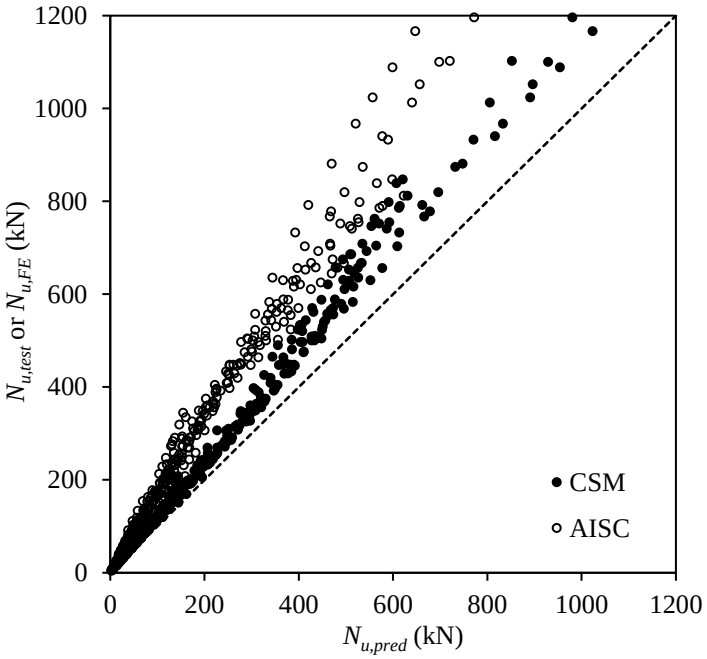

(b) In the 'u' orientation

Fig. 12. Comparison of combined loading test and FE results with CSM and AISC capacity predictions.